JOURNAL OF PROPULSION AND POWER
Vol. 23, No. 5, September–October 2007

Combustion Instability with a Single-Element Swirl Injector

Kevin Miller,* James Sisco,† Nicholas Nugent,† and William Anderson‡
Purdue University, West Lafayette, Indiana 47907

DOI: 10.2514/1.26826

A single injector element liquid rocket combustion experiment was designed and conducted to investigate the combustion dynamics of a gas-centered, liquid-swirled coaxial injector element. The oxidizer was a mixture of superheated water and oxygen, and kerosene was used as the fuel. The mean chamber pressure ranged from 2.14 to 2.38 MPa. The combustion chamber length was discretely varied between 25.4 and 88.9 cm to determine the dependence of combustion stability characteristics on resonant frequency and mode shape. Strong spontaneous instabilities were measured with peak-to-peak amplitudes of 0.69 to 1.38 MPa, and wave slopes on the order of 1000 MPa/s. The frequencies of the strongest instabilities ranged from 1184 to 1721 Hz. The most amplified modes ranged from the first longitudinal for the 38.1-cm chamber to the third longitudinal for the 88.9-cm chamber. One test, with a 25.4-cm chamber, was classically stable with pressure oscillation amplitudes less than 5% of the mean pressure. Resonant frequencies calculated with a model of the chamber acoustics compared well with measured values. For this injector, the data suggest that the observed stability behavior is a result of the combined effects of chamber mode shape and a driving combustion mechanism that limits the frequency range over which instability occurs.

I. Introduction

STABLE combustion is of prime importance to the successful design of high-energy density combustion systems. Liquid rocket engines, in particular, present one of the more challenging combustion systems in practice. Combustion instabilities are manifested by large pressure oscillations in the rocket combustion chamber with attendant high-amplitude dynamic thermal-structural loads. Initially small perturbations can be amplified by the coupling between energy release and pressure fluctuations, leading to catastrophic failures during engine operation.

Although a great deal of research regarding liquid rocket combustion instability has been conducted by industry and academia since the 1950s, a thorough understanding of the phenomenon has still not been obtained [1,2]. Instabilities in liquid engines are widely believed to result from a coupling of the complex and dynamic processes of injection, atomization, vaporization, mixing, and chemical reaction with a characteristic response of the gas dynamics in the combustion chamber. Because the injector dictates all of these parameters to a large extent, this component of the combustion system is the most important in affecting a change in the combustion dynamics. As such, it is necessary to determine the influence injector dynamics have on the stability of a combustion system.

This paper describes an experiment that has been designed with two primary objectives. The first objective addresses fundamental aspects of combustion stability and adds to the general engineering science by providing data that provide insight into the complex injector-induced dynamics. These data can be used, for example, to generally validate models of combustion instability, and directly determine basic parameters such as local sound speed, the degree of reflection at combustor boundaries, and the approximate axial location of the burning zone on which the burning admittance partially depends. In this paper a data set of mode shapes and amplitudes and power spectral density plots of spontaneous instabilities are provided for a well-described experiment, and compared to an acoustic analysis. A second objective is to explore an experimental tool that, when combined with analysis, could allow the stability rating of an injector design before a full-scale engine build. This combination of single-element test and analysis has been reported to yield accurate full-scale predictions [3]. This approach depends on the ability to sufficiently characterize the stability of the injector from a survey of its coupling behavior with longitudinal modes in a variable length combustor.

To study instability, the model combustor must exhibit some regime of unstable operation, therefore design considerations were made to "destabilize" the combustion process in this experiment. A gas-centered, fuel-swirl injector was tested in a variable length combustion chamber that was discretely varied between 25.4 and 88.9 cm (10 and 35 in.). The acoustic design of the injector–combustor combination was meant to sustain and amplify any resulting small pressure disturbances. Strong instabilities were easily excited and only one test, conducted with the 25.4 cm (10 in.) long chamber, was observed to be classically stable with peak-to-peak pressure oscillations less than 5% of mean chamber pressure. Pressure wave amplitudes of almost 900 kPa (130 psi) peak to peak and wave slopes on the order of 10^9 Pa/s were measured. Unstable frequencies ranged from 1184 to 1721 Hz, with unstable modes corresponding to the first, second, and third chamber modes. An acoustic analysis of the chamber is presented to demonstrate that, depending on chamber length, relatively damped modes can be driven to higher amplitudes than highly participatory modes. The results indicate that subscale tests can be used to detect and measure a combustion-determined bandwidth largely determined by the injector wherein the combustion dynamics will strongly couple with the chamber gas dynamics.

II. Background

A comprehensive review of experimental techniques used in examining combustion instability is presented in NASA SP-194 [3]. Although written over 30 years ago, the techniques described in SP-194 still largely describe the state of the art in U.S. rocket engine stability testing. The more recent review conducted by Dexter et al. [4] provides an excellent summary on the important issues of scaling the performance and stability characteristics between full-scale and

Presented as Paper 4298 at the 41st AIAA/ASME/SAE/ASEE Joint Propulsion Conference and Exhibit, Tucson, AZ, 10–13 July 2005; received 27 July 2006; revision received 8 January 2007; accepted for publication 19 January 2007.

*Graduate Research Assistant, School of Aeronautics and Astronautics; currently Propulsion Development Engineer, Space Exploration Technologies, El Segundo, CA.

†Graduate Research Assistant, School of Aeronautics and Astronautics. Student Member AIAA.

‡Assistant Professor, School of Aeronautics and Astronautics. Senior Member AIAA.

subscale hardware, as well as an interesting first glance at Russian injector stability rating methodology. Additional information on stability evaluation testing is also included in the AIAA monograph on combustion instability [5,6].

A. Scaling

Liquid rocket engine combustion instability has been investigated using a variety of combustor sizes from small-scale research experiments to full-scale engine tests. Full-scale engine testing is expensive and is not the preferred place to study combustion instability. Research or lab-scale combustors are focused on investigating combustion phenomena and chamber gas dynamics through detailed measurements. Full-scale component testing provides the most accurate representation of the engine design. Injection flows and chamber acoustics are all "full scale." The functional design of the chamber, however, may not allow for much instrumentation, and parametric studies such as injector element geometry require the fabrication and integration of multiple pieces of expensive hardware.

Subscale combustion diagnostic tests, often run at lower pressures, flow rates, and for shorter durations, are attractive because they are less costly in terms of hardware and test facility requirements, and are more amenable to a variety of measurement tools. Optical instruments and close-coupled high-frequency pressure transducers that may be incompatible with full-scale designs, especially those with regeneratively cooled chambers, are often feasible for use in a subscale experiment and may provide a wealth of physical data.

While some scaled experiments are focused on obtaining a better insight into the physics associated with combustion, others attempt to measure relative stability characteristics of an eventual full-scale design. Subscale test devices that have been used in the past include "two-dimensional" combustors and T-burners that attempt to provide similar acoustics to the full-scale chamber [1,3]. The basic premise behind these experiments is that the essential physics of the injector and combustor can be appropriately scaled or otherwise accounted for within the experiment. This is usually where subscale experiments fall short because it is extremely difficult to match the required similarity parameters that are pertinent to the performance and stability of the full-scale engine [3,7,8].

Tests with a single element of a multi-element injector have largely focused on characterizing the performance characteristics of a particular injector design [9–18]. A single-element experiment enables access to make detailed measurements of the mixing and reactions occurring in the injector flowfield. Single-element tests are usually conducted with coaxial injectors in reduced diameter chambers while maintaining a representative constant chamber length scale. Coaxial injector elements are most appropriate for single-element characterization as these injectors rely less on interactions between neighboring elements than do impinging designs. Experiments with certain full-scale single-element injectors show promise as a full-scale stability rating tool. It is hypothesized that the full-scale stability characteristics of so-called "pressure-sensitive" injector elements, where fluid mechanic effects that occur inside the injector (intraelement effects) dominate the combustion instability mechanism, may be revealed in a carefully designed single-element experiment.

B. Pressure-Sensitive Elements

A pressure-sensitive injector element is defined in the present context as an element that exhibits an appreciable response, in the form of energy release oscillations, as a result of local pressure fluctuations that propagate into the injector element. The pressure waves inside the element affect the internal flowfield and can modulate important processes such as compressible flow properties, atomization, and interpropellant mixing. This pressure-sensitive behavior occurs with injectors where the initial conditions for subsequent combustion in the chamber are largely determined inside the element itself.

Both shear and swirl-type bipropellant coaxial injectors often have a recess which allows the two propellants to mix before exiting the element. Experimental findings of both shear and swirl injectors have indicated that some amount of combustion also occurs within the element [17,19]. Because this initial region is recessed from the injector face, it is shielded from transverse waves and the intraelement dynamics respond only to local variations in the pressure. Thus it may be possible to characterize both fundamental and relative stability characteristics of the pressure-sensitive element through an experimental investigation of its response to longitudinal modes, which can be varied while maintaining fairly constant mean flow effects.

C. Approach

Russian researchers have claimed success in using pressure-sensitive single-element tests to determine full-scale engine stability characteristics [4]. Examination of the injector dynamics is carried out by matching the acoustics of the single-element combustion chamber to some representative full-scale engine chamber acoustic scale. Injector element geometry, volumetric flow rates, and equivalence ratio are cited as key parameters to maintain [4].

In the present experiment, detailed in [20], the chamber acoustics are varied by adjusting its length. This variable chamber length method has been employed in the past on several stability investigation programs [21–29]. Because longitudinal modes impose a pressure antinode at the injector face, the pressure sensitivity of an injector can presumably be examined independently of significant transverse velocity perturbations. To survey the injector response to transverse modes, the troublesome first few full-scale transverse acoustic modes are matched with longitudinal mode frequencies by varying the chamber length.

Because the natural acoustics of the system are varied by the adjustments to the chamber length, the chamber diameter may be held constant throughout the experiment. The chamber diameter should be selected to match a representative stream-tube area of the injector flow in a multi-element combustor. To alleviate any issues associated with scaling and to closely replicate the axial flowfield, the single-element design should be geometrically full scale and operate under its nominal flow conditions. The throat diameter is also set accordingly to provide a realistic mean combustion gas Mach number and chamber pressure.

D. Element Selection

An injector element based upon the Russian RD-170 injector was selected for the experiment [30,31]. This element is a gas-centered, liquid swirl coaxial injector that has seen extensive use in Russian liquid rocket engines (LREs), in particular, high pressure, oxygen–kerosene booster engines. The RD-170 injector element type was selected for the present study because its stability characteristics were reportedly examined through single-element testing [5,6]. In this experiment, a moderate pressure, decomposed hydrogen peroxide/kerosene element was tested. The use of the decomposed hydrogen peroxide as the oxidizer simulates the warm oxygen propellant in the oxidizer-rich staged combustion cycle (used with the RD-170) and allows for operational simplifications in test preparation and ignition since the JP-8 fuel can be autoignited.

A diagram of the injector element with a schematic description of its internal processes is given in Fig. 1. The injector consists of a central oxidizer post or injection tube that routes the gaseous oxidizer through the element axially. Liquid fuel is introduced into the injector through several tangentially drilled holes. Tangential injection imparts a circumferential velocity on the liquid and a swirling liquid sheet forms on the outer wall of the injector element. A collar shrouds the fuel sheet before it is exposed to the high velocity gas jet near the exit of the injector. In the region between the end of the collar and the injector face (the so-called mixing cup) the high velocity gas atomizes and entrains the swirling liquid sheet off of the wall and pulls the fuel toward the center of the injector.

This phenomenon of entrainment and mixing has been visually documented by Muss et al. [16]. These researchers tested numerous

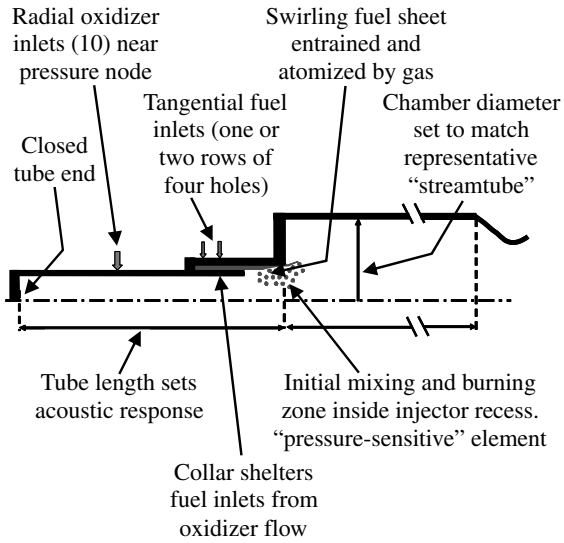

Fig. 1 Gas-centered, liquid swirl injector element.

gas-centered, liquid swirl, coaxial injector configurations in cold-flow and hot-fire test conditions. Their injectors varied slightly from the element in the present study and the RD-170 element in that there was no collar to shroud the tangential fuel inlets. Computational work performed by Canino et al. [32] also has captured this entrainment effect of the central, high velocity gas core. Combustion is believed to initiate inside the mixing cup, a claim that seems to be substantiated by experimental observations made by Cohn et al. [17]. Cheng et al. [33] performed computational fluid dynamics (CFD) analysis on these injectors and also found that under certain flow conditions that significant combustion can occur inside the element.

Of course, to study the phenomenon of instability it is desirable to have an experiment that shows some operational regime of instability. A survey of the literature reveals only one single-element experiment in which spontaneous unstable combustion was experienced [34]. Often, an artificial perturbation, such as a bomb, is required to force the combustor into an instability. These forced perturbations add a measure of complexity to the experiment as they are difficult to model and one must be able to extract the forcing function from the system response. Ideally, the combustor would exhibit linearly unstable behavior so that the development of pressure oscillations can be studied from their early, low amplitude stage.

Several design aspects were used to encourage pressure oscillations to develop in the combustor. The primary tactic was to acoustically couple the gaseous oxidizer post and combustion chamber. This acoustical coupling involved constructive interference by setting the oxidizer post length appropriately. The oxidizer post length was set during the initial design of the combustor with the intent of obtaining acoustic coupling with the second longitudinal mode of the combustion chamber at a chamber length of 63.5 cm (25 in.). This configuration serves as the baseline for the study. Minimal damping of upstream traveling pressure waves was created by providing an efficient flat reflective surface at the closed end of the oxidizer post. A short nozzle, less than 5% the length of the shortest chamber tested, was used to provide minimal damping of downstream traveling waves.

III. Experimental Apparatus

A schematic of the experimental single-element combustor is shown in Fig. 2. The combustion chamber consists of up to five discrete sections which were added or removed to allow for chamber length variation from 25.4 to 88.9 cm (10 to 35 in.). The head-end copper section was instrumented with up to four high-frequency pressure transducers and six ports for static pressure transducers. Four additional carbon steel sections were ported for further measurement access. The chamber diameter was 46.5 mm (1.83 in.).

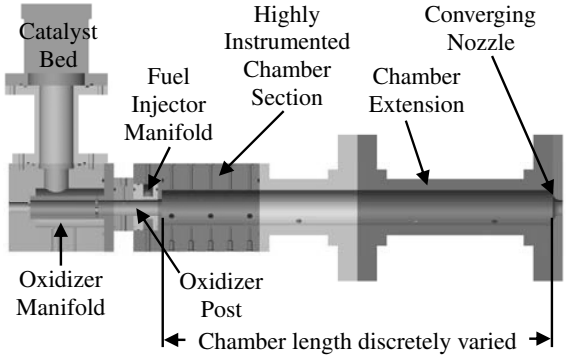

Fig. 2 Single-element combustor schematic.

A copper throat section closed out the chamber assembly. The throat diameter was 20.8 mm (0.82 in.) giving a chamber contraction ratio of 5, which was selected to ensure autoignition of the fuel by the hot gaseous oxidizer [35]. The 12.7 mm (0.5 in.) long converging nozzle was truncated at the throat.

The oxidizer was 90% by weight hydrogen peroxide, which was routed through a silver screen catalyst bed where it is decomposed into superheated oxygen and water vapor. When completely decomposed, the gaseous oxidizer consists of approximately 42% oxygen and 58% water vapor by weight and has a theoretical decomposition temperature 1029 K (1852°R) according to calculations performed using the NASA chemical equilibrium analysis code (CEA) [36]. The oxidizer enters an annular manifold and is introduced radially, with no swirl, into the oxidizer injector post near the midpoint of this 17.1 cm (6.72 in.) long, 2.05 cm (0.81 in.) diameter tube. A relatively large pressure drop (greater than 50% of the mean chamber pressure) is incurred across the radial inlets to decouple the manifold from flow disturbances occurring downstream in the combustion chamber and oxidizer post. The gaseous oxidizer flows axially through the tube and comes in contact with an annular sheet of swirling fuel that is stabilized on the outer injector wall at a diameter of 2.31 cm (0.91 in.). The JP-8 fuel sheet is initially sheltered from the gas flow by a 0.889 mm (0.035 in.) thick oxidizer post tip. Propellant mixing is initialized inside the element along the 5.08 mm (0.20 in.) recess between the end of the oxidizer post tip and the injector face.

Two fuel-swirl injector pieces were fabricated and tested under this study. A summary of injector parameters is given in Table 1. There were two primary differences between the two injectors. The first swirl injector, designated as fuel injector 1, had two rows of four tangentially drilled inlets, while the second injector, designated as fuel injector 2, had only a single row of four inlets. All holes in both injectors were 0.889 mm (0.035 in.) in diameter. The two rows in fuel injector 1 were spaced 4.3 mm (0.17 in.) apart in the axial flow direction and rotated 37 deg around the circumference of the injector with respect to each other. Fuel injector 2 had essentially half the flow area of fuel injector 1. The flow area reduction effectively increased the pressure drop across the injector by a factor of 4 at a given flow rate and therefore has more of a decoupling effect between chamber fluctuations and the fuel injection flow response. The second difference between the two swirl injectors was the length of the fuel injection holes. Fuel injector 1 had a longer injection hole passage

Table 1 Fuel injector design parameters

	Injector 1		Injector 2	
Flow rate, kg/s	0.073	0.091	0.073	0.059
No. of inlets	8	8	4	4
Inlet diameter, mm	0.889	0.889	0.889	0.889
Inlet length, mm	9.04	9.04	5.94	5.94
Inlet L/D	10.0	10.0	6.7	6.7
Film thickness, mm	0.33	0.33	0.20	0.20
Δp_{FJ}, kPa	228	352	876	579
Axial velocity, m/s	4.0	4.9	6.2	5.0
Circumferential velocity, m/s	23.2	29.0	46.0	37.5

9.04 mm (0.296 in.) than fuel injector 2 5.94 mm (0.125 in.) resulting in a larger length-to-diameter ratio. Estimations of the axial and circumferential film velocities and film thickness in the mixing cup were made assuming a quiescent environment and applying the principle of maximum flow through the swirl injector [37]. The fuel side injector pressure drop values Δp_{FJ} were derived from data averaged during each experiment.

Temperature measurements were made using omega type-*K* thermocouples. Piezoresistive strain-gage–type transducers, Druck models PMP 1260 and 4060, were typically sampled at 2 kHz and were used to measure the static or "dc" component of the pressure signal. Three different models of PCB integrated circuit piezoelectric (ICP) sensors were used to measure the dynamic or "ac" portion of the signal. These transducers respond within 20 μs to a physical rise in pressure making them well suited for high-frequency measurement. As many as five water-cooled, helium bleed pressure sensors, models 123A24 and 123M13, were used in the hot gas environment of the oxidizer manifold, oxidizer injector, and combustion chamber. One uncooled model 101A04 transducer was used in the fuel manifold, while another model 101A04 sensor with RTV coating was used in the chamber. In the fuel manifold the pressure transducer was flush mounted with the manifold wall. In the oxidizer manifold, oxidizer post, and combustion chamber, the high-frequency transducers were mounted in a small recess to provide further protection from hot gases. The natural frequencies of the pressure ports were calculated assuming the port to be a simple Helmholtz resonator [1]. Up to eight channels of high-frequency data were simultaneously sampled at 500 kHz throughout the test program and the signals were not filtered by any hardware device during data acquisition. A National Instruments LabVIEW virtual instrument program was used to control all valves in the system as well as the electronically controlled, dome-loaded tank regulators. Cavitating venturis upstream of the catalyst bed and the fuel manifold maintained constant oxidizer and fuel flow rates, respectively.

IV. Experimental Results

A total of 10 combustion experiments were performed during the study. Because the main experimental objective was to measure how the injector element responds to changes in the natural system acoustics, a length variation survey was performed at nearly constant mean flow rate conditions. Tests were also performed to investigate the effects of the fuel injector design, mixture ratio, and the repeatability of the data. A total of three different fuel flow rate conditions were run while the oxidizer injection flow rate was held within a tight band between 0.459 and 0.477 kg/s (1.01 and 1.05 lb/s). Static temperature and pressure measurements were taken within the oxidizer post and used in a one-dimensional, plug flow analysis to calculate gas injection parameters within the injector. The gas side injection velocity and density were estimated to range from 171 and 198 m/s (560 to 650 ft/s) and 5.8 and 6.6 kg/m^3 (0.36 to 0.41 lb/ft^3), respectively, over the narrow variation of oxidizer flow conditions. The average gas injection Mach number was 0.28 and the acoustic speed was 668 m/s (2190 ft/s). The theoretical value of the combustion chamber Mach number and acoustic speed was 0.12 and 1090 m/s (3560 ft/s), respectively, again referring to CEA calculations [36].

Table 2 lists a summary of the operating conditions and results for the tests that are the focus of this paper. Each test is given a mnemonic label with the first two digits defining the chamber length in inches, the letter indicating the fuel flow rate (L = low, D = design, H = high), and the last digit indicating the fuel injector number. A test label appended with the letter "r" indicates that it was a repeat of a prior test condition. Therefore, test 25D2 was the only test performed with the 63.5 cm (25 in.) chamber at a flow rate of 0.073 kg/s through fuel injector 2. The operating conditions and performance parameters listed in Table 2 for each test, columns three through nine, are arithmetic means (sum of samples divided by number of samples) calculated over a 200 ms time slice during the steady-state portion of each bipropellant test (this time slice is discussed in more detail below).

High-amplitude instabilities were spontaneously excited in nine of the ten tests reviewed. Test 10D1 with the shortest chamber length was the only test in which combustion was classically stable according to the Chemical Propulsion Information Agency (CPIA) guidelines [38]. Pressure oscillations were under 5%, mean to peak, of the mean combustion chamber pressure of 2.4 MPa. All other tests were unstable at a frequency that correlated well with the natural acoustics of the combustion system. Test 35D1 has two entries in Table 2 as it was initially unstable at 1721 Hz before transitioning to a lower acoustic mode at 1233 Hz. The mean-to-peak pressure oscillations p' estimated from dynamic pressure data measured 1.27 cm (0.5 in.) from the injector face are listed in the last column of Table 2. This location was chosen due to its proximity to the injector face and thus an assumed pressure antinode. A procedure for calculating p' is described below.

Figure 3 shows the typical character of an unstable test. The static chamber pressure was measured 6.4 cm (2.5 in.) downstream of the injector face, while the high-frequency oscillating pressure was measured 1.3 cm (0.5 in.) from the injector face. At reference time $t = 0$ s, the main fuel valve is opened initiating fuel flow from the propellant tank to the fuel manifold. Around $t = 0.7$ s, the fuel is injected into the combustor and ignited by the hot oxygen vapor already flowing through the combustor. The decomposed peroxide products flowing at their nominal rate cause the 800 kPa (120 psi) backpressure in the chamber at the start of fuel flow. After a violent fuel ignition event at $t = 0.7$ s, the chamber pressure rises steadily and the dynamic portion of the pressure signal indicates only low-level background combustion noise. Near $t = 0.85$ s, where the chamber pressure starts to level off, an instability grows and eventually reaches a limit-cycle amplitude. The instabilities produced an audibly loud, high-pitched tone. Typically, the fuel valve was only opened for 1.5 and 2 s before being shut off.

A representative 45 ms slice of unfiltered dynamic pressure data from test 25D1r is shown in Fig. 4. The predominant high-frequency oscillations are of wave amplitudes as high as 900 kPa (130 psi). A closer look at an ensemble of waves in test 25D1r presented in Fig. 5 shows the steep-fronted nature of the waves as captured 1.3 cm

Table 2 Test summary conditions and results

Test	Chamber length, cm	Ox flow rate, kg/s	Fuel flow rate, kg/s	O/F	η_{C^*}	p_c, MPa	Δp_{OJ}, MPa	ΔP_{FJ}, MPa	Unstable frequency, Hz	p', kPa
10D1	25.4	0.461	0.073	6.3	94.2	2.38	1.01	0.132	stable	13
15D1	38.1	0.462	0.074	6.2	87.4	2.21	1.24	0.260	1502	295
20D1	50.8	0.479	0.073	6.5	86.3	2.21	1.73	0.179	1184	151
20D1r	50.8	0.464	0.074	6.3	90.1	2.29	1.14	0.170	1184	167
25H1	63.5	0.479	0.092	5.2	83.4	2.16	1.86	0.341	1672	431
25L2	63.5	0.466	0.058	8.0	88.4	2.19	1.18	0.491	1648	156
25D1	63.5	0.478	0.074	6.5	83.8	2.14	1.83	0.225	1709	328
25D1r	63.5	0.459	0.074	6.2	87.3	2.19	1.16	0.165	1660	258
25D2	63.5	0.461	0.073	6.3	86.5	2.18	1.19	0.721	1672	266
35D1 (early)	88.9	0.464	0.074	6.3	86.0	2.18	1.17	0.166	1721	244
35D1 (late)	88.9	0.463	0.074	6.3	87.7	2.22	1.17	0.160	1233	148

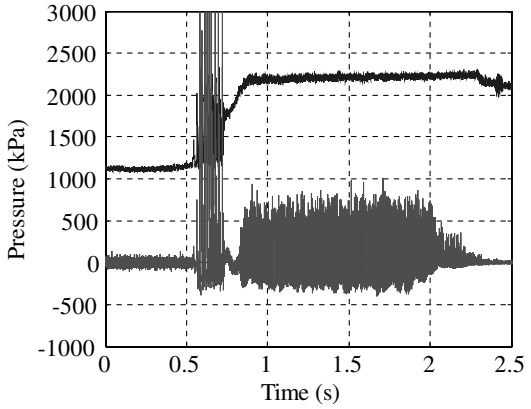

Fig. 3 Static (upper) and dynamic (lower) pressure signals measured during unstable combustion test 25D1r.

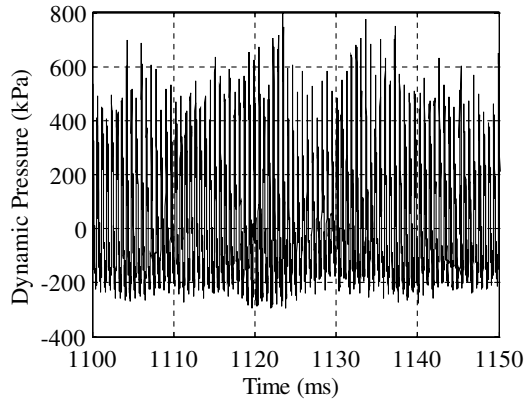

Fig. 4 Dynamic pressure signal during unstable combustion test 25D1r (50 ms scale).

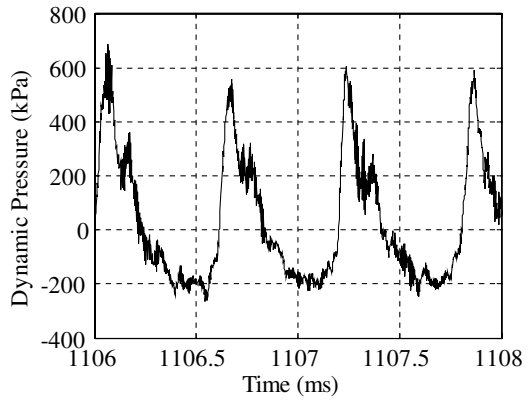

Fig. 5 Dynamic pressure signal during unstable combustion test 25D1r (2 ms scale).

downstream of the injector face. The initial peak captures the pressure wave as it arrives at the transducer and is followed by a second peak due to a wave reflection off the injector.

To compare the resulting instabilities in each test, the dynamic pressure data are analyzed over a representative time frame of limit-cycle instability. The specific time frame selected starts approximately 0.3 s after the last ignition spike and lasts for 200 ms. Qualitatively, this appeared to be an appropriate time to compare across all tests. This allowed enough time for the instability to transition into a fully developed oscillation, while ending before thermal drift effects would saturate any of the pressure sensor output signals. The raw pressure data were low pass filtered at 25 kHz using a digital Butterworth filter and subsequently downsampled by a factor of 10, that is, every 10th data point was retained for analysis. A power spectral density (PSD) was calculated over this selected frame using a discrete Fourier transform. The frequency bin resolution for the PSD was 12.2 Hz. Figure 6 shows the resulting power spectrum plots for several tests. The power of each acoustic peak up to the fourth harmonic was integrated to estimate the strength of the pressure oscillation. The integration was performed over the full width of the peak that was above half the maximum power value. A root-mean-square (rms) pressure value of the oscillation was calculated by summing the peak power values. Multiplying the rms pressure oscillation by the square root of 2 yields the estimated average mean-to-peak pressure oscillation value p'. The values of p' for each experiment are reported in Table 2.

A. Chamber Length Survey

Figure 6 shows the power spectral data for several tests conducted during the chamber length variation survey. All these tests were performed with the eight-hole fuel injector and near the design fuel flow rate. The dynamic pressure data shown in Fig. 6 were measured in the combustion chamber 1.3 cm downstream of the injector face. The power spectrum of the single stable experiment is shown in Fig. 6a. The wideband peaks near 2000 and 4000 Hz are consistent with the combustion chamber first and second longitudinal modes, respectively. When the chamber was lengthened beyond 25.4 cm (10.0 in.), a transition to unstable combustion ensued.

Power spectral plots of the steep-fronted waves show the fundamental oscillation frequency along with several higher harmonic peaks. Test 15D1 was unstable at 1502 Hz near the first longitudinal mode of the 38.1 cm (15.0 in.) chamber as shown in Fig. 6b. When the chamber length was increased to 50.8 cm (20.0 in.), the oscillations persisted near the first longitudinal mode frequency at 1184 Hz as shown in Fig. 6c. Also apparent in Fig. 6c are underlying peak frequencies near 2000 and 3000 Hz. A transition to a higher mode, near the chamber second longitudinal, was experienced when the chamber length was further increased. Figure 6d is the power spectrum of test 25D1r performed with the 63.5 cm (25.0 in.) chamber. An additional test was run with an 88.9 cm (35 in.) long chamber. Test 35D1 was initially unstable near the chamber third harmonic at 1721 Hz before transitioning to the lower second mode of 1233 Hz at about $t = 1.3$ s into the test. The early and late periods of the limit cycle instabilities experienced in test 35D1 are shown in Figs. 6e and 6f, respectively. In both plots of test 35D1, it can be seen that the 1721 and 1233 Hz modes were present at some amplitude throughout the test.

Repeatability in combustor operation was investigated at two different chamber lengths. Two tests, labeled as 20D1 and 20D1r in Table 2, were run at a chamber length of 50.8 cm (20 in.). As Table 2 shows the calculated mass flow rates, mixture ratios, and fuel injector pressure drops of both tests were approximately identical, within 3.5%. There was a significant decrease in the oxidizer injector pressure drop between tests 20D1 and 20D1r due to an increase in the oxidizer injector orifice diameter. This modification was driven by the need to reduce the oxidizer manifold pressure to within design limits of the catalyst bed. This modification was assumed to have negligible impact on the oxidizer mass flow rate due to the high Mach number of the oxidizer leaving the injection orifices, approximately 0.8. At high Mach numbers acoustic fluctuations propagating from the oxidizer post to the oxidizer manifold will be significantly damped, and will therefore have a minimal effect on the oxidizer mass flow rate. This is confirmed by the fact that the unstable frequencies, determined through PSDs, were identical for both tests run at this chamber length. In addition, the mean-to-peak pressure oscillations, also determined through the calculated PSDs, are within approximately 10%.

As previously mentioned two tests were also run at a chamber length of 63.5 cm (25 in.) to investigate repeatability in combustor performance, shown as 25D1 and 25D1r in Table 2. In these tests the mass flow rates and mixture ratios were within 4.5% and, as with the 50.8 cm chamber, the oxidizer injector had been modified between tests 25D1 and 25D1r resulting in a 30% difference in oxidizer injector pressure drop. There was also a large difference in fuel

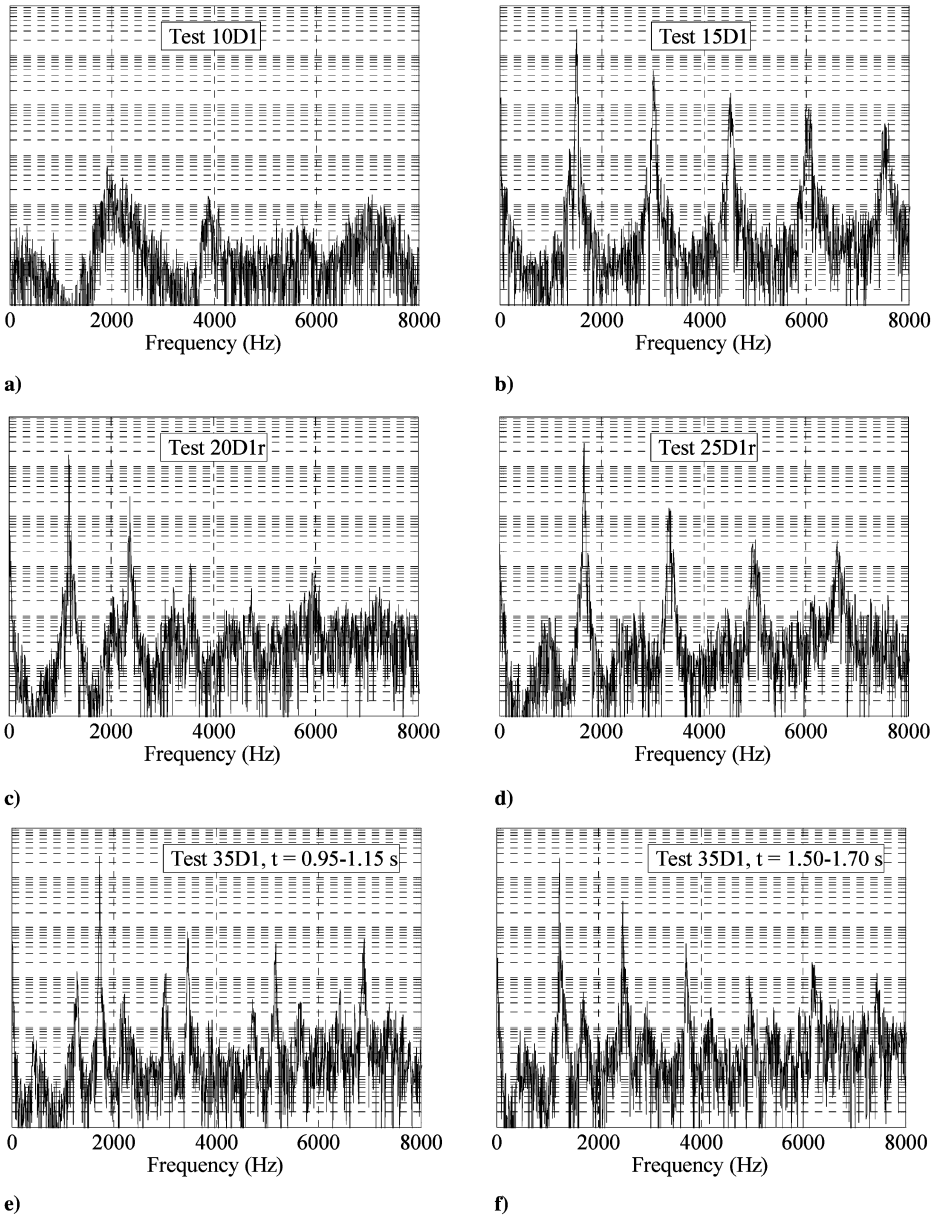

Fig. 6 Representative limit cycle power spectra at each tested chamber length from combustion chamber dynamic pressure measurement located 1.3 cm (0.5 in.) from injector face.

injector pressure drop, approximately 30%, between these two tests despite the fact the fuel injectors and calculated fuel mass flow rates were identical. The average chamber pressure used to calculate the pressure drop for test 25D1 is 0.05 MPa lower than that for test 25D1r (there was only a 0.01 MPa difference in the fuel manifold pressure between the two tests). It is unclear as to the specific reason for this difference, it may be a result of several factors combined, but there is nothing in the data to indicate the injector should have performed any differently than in test 25D1r. Analysis of measured high-frequency data from these tests shows that the unstable frequencies are within 3%, however, the calculated mean-to-peak pressure oscillation is almost 30% lower in test 25D1r than 25D1. It would appear that there are mixed results regarding the repeatability of the pressure oscillations in the chamber between the 50.8 and 63.5 cm chamber lengths, perhaps suggesting that further testing may be required to fully characterize repeatability during unstable combustor operation.

B. Fuel Injector Comparison

Tests 25D1, 25D1r, and 25D2 provide a comparison between the two fuel injectors with different injection pressure drops. All tests were unstable near the same frequency. Tests with fuel injector 1 were unstable at 1660 and 1709 Hz while fuel injector 2 was unstable at 1672 Hz. The estimated average mean-to-peak pressure oscillation amplitudes p' for these three experiments are reported in Table 2. As previously mentioned there was a 30% difference in the calculated p' between tests 25D1 and 25D1r, however, the calculated p' for tests 25D1r and 25D2 agree to within approximately 3.5%.

It is difficult to make conclusions about the steady-state performance of the injector when such vigorous instabilities persist throughout the test. In spite of this, the mean pressure values are calculated, by an arithmetic mean, at several locations during the unstable tests to gauge the pressure profile along the injector and combustor axis. Figure 7 shows the resulting pressure profiles of the two fuel injectors where ◆ denotes measurements from test 25D1r run with injector 1 and ■ denotes measurements from test 25D2 run with injector 2. The first measurement on the left was taken inside the oxidizer tube downstream of the radial inlets. The remaining measurements were made in the chamber. There is a noted increase, or recovery, in the static pressure of the flow upon leaving the 2.31 cm (0.908 in.) diameter injector and entering into the 4.65 cm (1.83 in.) chamber diameter. This pressure recovery behavior is common to all tests. The pressure appears to be fairly constant between the 11 cm (4.5 in.) and 46 cm (18 in.) locations on test 25D2.

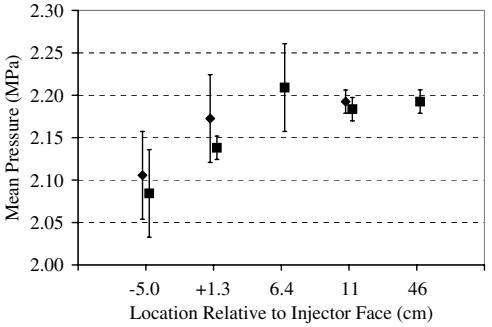

Fig. 7 Measured static pressure profiles for tests 25D1r ◆ and 25D2 ■ (error bars also shown).

This phenomenon is not a consequence of injector performance, but rather a result of the flow expanding to form a recirculation zone downstream of the injector face, which is analogous to flow over a rearward-facing step. The axial point of static pressure recovery corresponds approximately to the flow reattachment point, which typically occurs five step heights downstream of the injector face for a reacting flow [35]. In this experiment the step height, or injector face width, is 1.10 cm (0.433 in.) which places the reattachment point at approximately 5.50 cm (2.17 in.) downstream of the injector face. The measured data from both tests 25D1r and 25D2 confirm that the static pressure profile is approximately flat downstream of the theoretical reattachment point, within 2.5%, from the 6.4 cm (2.5 in.) to the 46.0 cm (18 in.) measurement locations in the chamber.

V. Data Analysis

An acoustic analysis was developed, using a method outlined in Kinsler et al. [39], to gain a better understanding of the fundamental acoustics of the coupled oxidizer post/combustion chamber system and to help interpret experimental data. It is important to point out that the model is not capable of providing stability predictions in the form described here. In the analysis it is assumed that the propagation of sound through the fluids in the system can be modeled by the linear, lossless wave equation. In addition, it is assumed that sound propagates as one-dimensional, plane waves. The system is broken up into two discrete sections: the oxidizer post (section 1) and combustion chamber (section 2), each with its own mean density $\bar{\rho}$, mean sound speed $\bar{a}$, geometric length L, and cross-sectional area S. A schematic of the system indicating each of these parameters is shown in Fig. 8; note that the origin of the axial coordinate x is placed at the injector face. Effects due to mean flow, entropy waves, liquid injection, vaporization, and combustion are not considered in this analysis; rather it is assumed that the gas properties immediately take on those of the combustion products downstream of the injector face, in section 2. Upstream of the injector face, in section 1, the gas properties take on those of decomposed hydrogen peroxide.

The wave equation is solved in sections 1 and 2 for acoustic pressure subject to the admittance boundary conditions Y_{L1}, Y_{01}, Y_{02}, and Y_{L2}. Admittance Y is defined as the ratio of acoustic volume velocity to acoustic pressure where acoustic volume velocity is defined as acoustic velocity multiplied by cross-sectional area. The linear Euler equation is used to relate the acoustic velocity to acoustic pressure [39]. At the injector face $x = 0$, the admittance boundary conditions Y_{01} and Y_{02} are set equal to each other. The head end of the oxidizer post $x = -L_1$ is considered a rigid, fully reflective wall and its admittance is assumed to be zero, $Y_{L1} = 0$. The nozzle is also assumed to be a rigid, fully reflective wall and its admittance is also set equal to zero, $Y_{L2} = 0$. This is a reasonable approximation of the highly reflective short nozzle used in this experiment. A system of equations is generated using these boundary conditions which can be solved to determine the acoustic resonance frequencies of the coupled system for any combination of geometry and gas properties. The mode shapes, in terms of acoustic pressure and/or velocity, can also be plotted for any frequency subject to the admittance boundary conditions outlined above and specified geometry and gas properties.

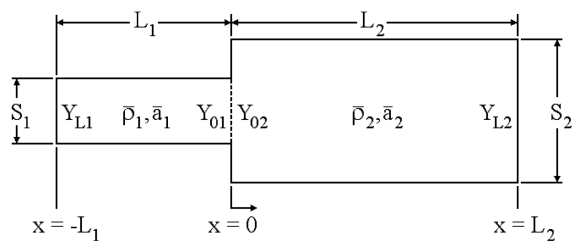

Fig. 8 Schematic detailing geometry and boundary conditions used in acoustics model.

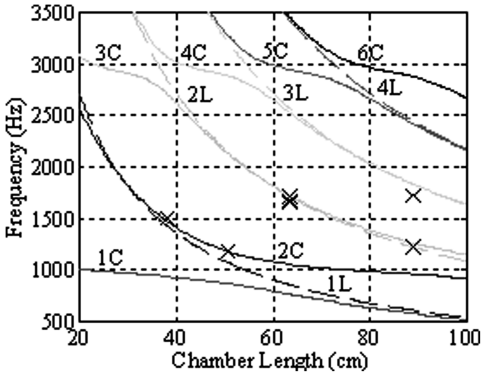

Fig. 9 Coupled oxidizer post/combustion chamber resonance frequencies for post length of 17.1 cm (6.72 in.) and chamber length variation from 20 to 100 cm (7.9 to 39.4 in.). Solid lines represent coupled modes, dashed lines represent chamber modes, and X's indicated measured frequency of highest amplified mode.

A plot of the resonance frequencies based on combustion chamber length for an oxidizer post length of 17.1 cm (6.72 in.), which was used in the experiment, is shown in Fig. 9. In this figure the first six coupled system resonance frequencies are plotted as solid lines and are denoted by "C." The dashed lines represent the first four longitudinal modes, denoted by "L," based on combustion chamber properties and geometry alone, and are calculated from the following equation:

$$f_n = \frac{n\bar{a}_2}{2L_2} \quad \text{where } n = 1, 2, 3, \ldots \tag{1}$$

Here f_n denotes the nth longitudinal mode frequency in hertz, while $\bar{a}_2$ and L_2 represent the chamber sound speed and chamber length, respectively. The sound speeds and densities used in the calculations are based on theoretical conditions in the chamber and post. The "X" marks in Fig. 9 denote the frequency of the largest peak in the power spectral density generated from measured test data at each chamber length calculated from pressure data measured 1.27 cm (0.5 in.) from the injector face. At a chamber length of 88.9 cm (35 in.) both observed frequencies are shown (tests run at off-design fuel mass flow rates are not reflected in this figure). From this figure it is apparent that the combustion chamber is the dominant component of the acoustic system as the coupled modes follow the chamber modes very closely over a large range of chamber lengths. However, at certain lengths and frequencies the coupled modes deviate from those of the chamber and actually transition to higher chamber modes. This can be seen in the second coupled mode 2C, at a chamber length of 38.1 cm (15 in.) and frequency of about 1500 Hz. The 2C mode begins to deviate greatly from the first longitudinal chamber mode 1L as the chamber length increases and begins to approach the second longitudinal chamber mode 2L. In fact, the measured unstable frequency from the test run at a 50.8 cm (20 in.) chamber length is closer to that of the 2C mode than the 1L, as shown in Fig. 9.

It is also interesting to note that the calculated coupled resonance frequencies are not necessarily integer multiples of one another as they are for simple chamber longitudinal modes. For instance, at a chamber length of 50.8 cm (20 in.) the first four coupled resonance frequencies are 870, 1182, 2129, and 2883 Hz. The calculated PSD

Table 3 Comparison between calculated modes and measured unstable frequencies

Test	Chamber length, cm	Measured unstable frequency, Hz	Chamber only acoustic analysis [Eq. (1)]			Coupled acoustic analysis (Fig. 9)		
			Closest mode	Predicted frequency, Hz	Deviation, %	Closest mode	Predicted frequency, Hz	Deviation, %
10D1	25.4	stable	——	——	——	——	——	——
15D1	38.1	1502	1L	1426.8	5.01	2C	1477.3	1.64
20D1	50.8	1184	1L	1070.1	9.62	2C	1182.3	0.14
20D1r	50.8	1184	1L	1070.1	9.62	2C	1182.3	0.14
25D1	63.5	1709	2L	1712.2	0.19	3C	1724.3	0.90
25D1r	63.5	1660	2L	1712.2	3.14	3C	1724.3	3.87
25D2	63.5	1672	2L	1712.2	2.40	3C	1724.3	3.13
35D1 (early)	88.9	1721	3L	1834.5	6.60	4C	1838.6	6.83
35D1 (late)	88.9	1233	2L	1223.0	0.81	3C	1267.3	2.78

from measured data at 1.27 cm (0.5 in.) in the combustion chamber from test 20D1r, Fig. 6c, shows a primary peak at a frequency of 1180 Hz with corresponding lesser peaks at integer multiples of 2370, 3550, and 4750 Hz. This phenomenon has also been measured at all other unstable chamber lengths. It is believed that this is a nonlinear acoustic effect whereby acoustic energy is transferred to the harmonics, integer multiples, of the fundamental mode. This may be confirmed by the presence of a peak at a frequency of approximately 2040 Hz in the same PSD, see Fig. 6c, of lesser magnitude than the harmonic at 2370 Hz. This peak is very close to the 3C mode frequency of 2111 Hz.

A comparison of the measured unstable frequencies to the closest resonance frequencies predicted by the coupled acoustic model and Eq. (1) for each chamber length is shown in Table 3 (tests run at off-design fuel mass flow rates are not reflected in this table). These results must be viewed with some reservation as the sound speeds in the oxidizer post and combustion chamber were estimated from equilibrium chemistry calculations. Using these gas properties the resonance frequencies predicted by the coupled acoustic model more accurately approximate those measured during the experiment than Eq. (1) especially at the shorter chamber lengths. This is a result of the deviation of the coupled modes from traditional longitudinal modes, as was described above. Based on these results there is some evidence that the acoustics of the coupled system are influenced by the oxidizer post.

The oxidizer post essentially acts as an acoustic resonator and can either damp or amplify the amplitude of acoustic pressure oscillations in the combustion chamber. A potential consequence of this is that the post could influence combustion dynamics and possibly dictate the frequency of unstable operation. The mode shapes calculated using the acoustic model described above were used to quantify the damping effect of the post for the first four longitudinal modes, calculated using Eq. (1), at each chamber length.

Before describing the results of this investigation it is useful to analytically derive a relation for the oxidizer post length necessary for minimum and maximum damping of the chamber acoustic modes. Maximum damping of the chamber mode will occur when the time it takes for an acoustic pressure wave to propagate up and down the post is equal to half the period of the chamber mode. Assuming a pressure antinode at the upstream end of the combustion chamber, maximum damping will occur when a compression at the post exit coincides with a rarefaction at the chamber head end. These positive and negative maximums essentially cancel each other, thereby damping the amplitude of the oscillation. On the other hand, minimum damping will occur when the propagation time of a pressure wave up and down the post is exactly equal to the period of the chamber mode, that is, a pressure maximum at the post exit coincides with a pressure maximum at the post head end.

The oxidizer post length L_1 required for maximum chamber mode damping is

$$\frac{L_1}{\lambda_1} = \frac{1}{4} \tag{2}$$

where the wavelength of the pressure oscillation in the post is defined as follows:

$$\lambda_1 = \frac{\bar{a}_1}{f_n} \tag{3}$$

and where $\bar{a}_1$ is the sound speed in the oxidizer post and f_n is the chamber mode frequency of interest. Similarly the oxidizer post length for minimum chamber mode damping is

$$\frac{L_1}{\lambda_1} = \frac{1}{2} \tag{4}$$

As previously mentioned the oxidizer post length was designed such that the condition for minimum damping, Eq. (4), was satisfied for the frequency corresponding to the second longitudinal mode of the 63.5 cm (25 in.) chamber. As it turned out all tests run at this chamber length were unstable. An important question to ask is whether or not the least damped condition is necessary for instability, which has generally been the assumption for this pressure-sensitive injector element. To answer this question the acoustic model was used to evaluate the level of acoustic damping provided by the oxidizer post for each longitudinal frequency of the off-baseline chamber lengths.

An example of the damping effect of the post is illustrated by the mode shapes for the 50.8 cm (20 in.) chamber. The first (1070 Hz) and second (2140 Hz) longitudinal modes at this chamber length are plotted over one period in time (to show extents) in Fig. 10. The absolute magnitude of acoustic pressure in Fig. 10 is arbitrary; therefore the ratio of the maximum acoustic pressure in the combustion chamber, which may or may not be at the injector face, to the maximum in the oxidizer post, which is always at the head end, is used to compare the damping effect between modes. This ratio is referred to from here on as the acoustic pressure ratio, APR. Figure 10a shows the first longitudinal mode is highly damped in the combustion chamber with an acoustic pressure ratio of 0.187. The predicted value of L_1/λ_1 is equal to 0.274 in this case, which is very close to the most highly damped value of 0.25 shown in Eq. (2). On the other hand, the second longitudinal mode, Fig. 10b, is minimally damped in the chamber with an APR of 0.957. In this case the predicted value of L_1/λ_1 is equal to 0.547, which is very close to the least damped value of 0.50 shown in Eq. (4). A summary of APR and L_1/λ_1 values for each of the first four longitudinal modes at each chamber length is shown in Table 4.

Considering the level of acoustic damping provided by the oxidizer post for the two modes shown in Fig. 10 for the 50.8 cm (20 in.) chamber length, one would expect the 2L mode (2140 Hz) to be more unstable because it is very close to the least damped condition. However, as Table 3 shows, the tests run at this chamber length, 20D1 and 20D1r, were unstable at 1184 Hz, which is much closer in frequency to the 1L mode (1070 Hz) than the 2L. This is a surprising result in that the combustion process chose to couple with the weaker acoustic mode. Similar results can be seen at chamber lengths of 25.4 cm (10 in.) and 88.9 cm (35 in.). The 1L mode for the 25.4 cm (10 in.) chamber is at a frequency 2140 Hz (essentially the 2L of the 50.8 cm chamber since it is half the length) and is minimally damped in the combustion chamber with an APR of 0.957, shown in Table 4. Even though there is a strong acoustic mode available for the

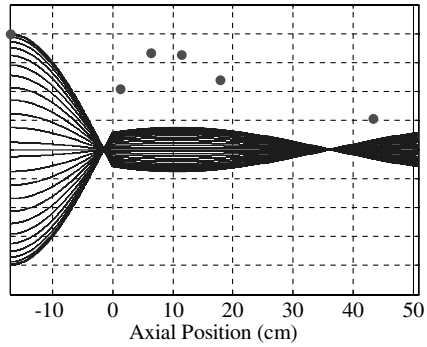

a)

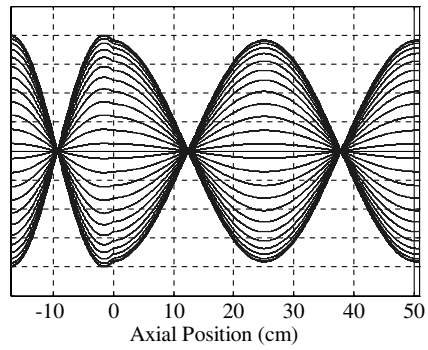

b)

Fig. 10 a) Comparison between mode shape calculated by acoustic model for 1L mode of 50.8 cm (20 in.) chamber (1070 Hz) and measured dynamic pressure profile from test 20D1r ● and b) calculated mode shape for 2L mode (2140 Hz) of 50.8 cm (20 in.) chamber.

combustion process to couple with, the test run at this chamber length, 10D1, was actually stable. There was, however, a low amplitude peak at approximately 1900 Hz (see Fig. 6a) indicating that the 1L mode was somewhat excited during the test.

The measured dynamic pressure profile from test 20D1r is also compared to the calculated mode shape for the 1L mode (1070 Hz) of the 50.8 cm (20 in.) chamber in Fig. 10a. A more complete description of the generation of this plot can be found in Sisco et al. [40]. The general shape of the pressure profile and mode shape agree fairly well; however, the amplitude in the combustion chamber is considerably higher in the measured data. It should be pointed out that these measured amplitudes are estimated from oscillations seen during the limit cycle portion of the instability. Thus one might expect there to be considerable amplification of the pressure oscillation amplitude from its amplitude when considering acoustics alone during an instability.

Table 4 Damping effect of the oxidizer post on chamber longitudinal modes

Mode	f_n, Hz	APR	L_1/λ_1
Chamber length = 25.4 cm (10 in.)			
1L	2140.2	0.957	0.547
2L	4280.4	0.833	1.094
3L	6420.6	0.638	1.641
4L	8560.8	0.395	2.188
Chamber length = 38.1 cm (15 in.)			
1L	1426.8	0.666	0.365
2L	2853.6	0.174	0.729
3L	4280.4	0.833	1.094
4L	5707.2	0.967	1.459
Chamber length = 50.8 cm (20 in.)			
1L	1070.1	0.187	0.274
2L	2140.2	0.957	0.547
3L	3210.3	0.441	0.821
4L	4280.4	0.833	1.094
Chamber length = 63.5 cm (25 in.)			
1L	856.1	0.226	0.219
2L	1712.2	0.925	0.438
3L	2568.2	0.563	0.656
4L	3424.3	0.713	0.875
Chamber length = 88.9 cm (35 in.)			
1L	611.5	0.564	0.156
2L	1223.0	0.398	0.313
3L	1834.5	0.981	0.469
4L	2446.0	0.711	0.625

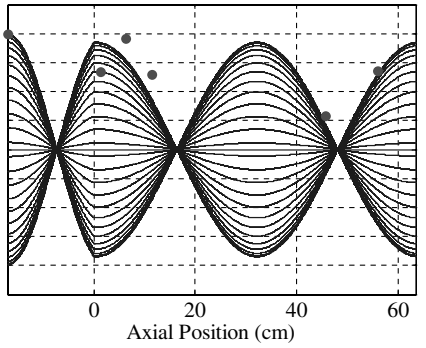

Fig. 11 Comparison of dynamic pressure data from test 25D1r (unstable at 1660 Hz) and mode shape calculated by acoustic model for input frequency of 1712 Hz.

Better agreement can be seen in the measured and predicted pressure profiles for a configuration satisfying the least damped condition. A comparison between the measured dynamic pressure profile for test 25D1r at a chamber length of 63.5 cm (25 in.) and the calculated mode shape at the chamber 2L frequency (1712 Hz) is shown in Fig. 11. The figure shows that there is good qualitative agreement between the mode shape calculated by the model and the measured dynamic pressure profile. It is interesting to note that the maximum dynamic pressure was measured at the head end of the oxidizer post and the maximum value measured in the chamber is found 6.4 cm (2.5 in.) from the injector face. This behavior is consistent with all unstable chamber lengths [40], suggesting that a pressure antinode forms at the post head end and approximately 6.4 cm (2.5 in.) downstream of the injector face during unstable operation. Coincidently, or perhaps not, the location of maximum dynamic pressure coincides with the estimated location of reattachment length of the recirculation zone downstream of the injector face.

In the test run at a chamber length of 88.9 cm (35 in.) unstable combustion began at a frequency of 1721 Hz, which is close to the strong 3L mode of 1834.5 Hz with an APR of 0.981. The 3L instability transitioned to the 2L mode at 1233 Hz at the end of the limit cycle portion of the test. The 2L mode is more damped in the chamber at an APR of 0.398. Therefore, during this test the combustion started unstable at a minimally damped acoustic mode, but chose to move to a more damped mode during the test, possibly indicating an effect of the combustion process preferentially driving the more damped mode. The preference could be based on a time scale effect, or be due to more efficient spatial coupling between the 2L mode and the energy release. It is also interesting to note that the 3L instability in this test also presented the greatest difference between measured and calculated mode frequencies (see Table 3). Based on these results it is clear the acoustic modes couple with the combustion process to select the dominant unstable mode. However, the presence of a strong pressure antinode, a characteristic of the minimum damping condition, near the injector does not appear to be necessary or sufficient to drive combustion instability.

VI. Conclusions

An experiment was designed to quantitatively characterize the combustion dynamics of a single gas-centered, fuel-swirled injector element. The combination of the injector and combustion chamber was designed to promote unstable operation at certain conditions. The experimental design was proven to be capable of developing

spontaneous combustion instabilities over a wide range of well-defined frequencies, and to provide model validation data including mode frequency and shape, and limit cycle amplitudes.

The model combustor was tested at five different lengths, from 25.4 to 88.9 cm, by adding a cylindrical section to the combustion chamber upstream of a short nozzle used to reduce acoustic losses. Both stable and unstable operations were exhibited throughout the chamber length survey. With increasing chamber length, distinct transitions from stable to unstable behavior and from lower to higher modes were experimentally observed. The pressure oscillations comprised high-amplitude, steep-fronted waves and reached limit cycle amplitudes that approached 50% of mean chamber pressure. Results from tests with different fuel injectors were similar suggesting second-order fuel delivery effects for the configuration as tested.

A model of the combined injector-chamber acoustics predicted the resonant frequencies of the highest amplitude modes well. When the dominant instabilities were either first or second longitudinal modes, the predicted frequencies were within 4% of the measured frequencies. When the dominant instability was a third longitudinal mode, the predicted frequency was within 6% of the measured frequency. It is speculated that the larger discrepancy is due to heat addition occurring closer in space to the pressure node of the higher mode. The acoustic model results also demonstrated that the least damped acoustic modes according to calculation were not necessarily the most unstable modes determined by experiment.

The experimental results indicate that, in this model combustor, this particular injector element is not prone to excite instabilities at fundamental frequencies below 1050 Hz and above 1810 Hz. These results suggest the presence of a driving combustion mechanism and associated unsteady heat addition with a certain range of space and time characteristics. The temporal and spatial aspects of heat addition couple with mode shape to select the most amplified mode. These results further suggest that it is possible to use subscale experimental results to design a full-scale injector that possesses temporal and spatial combustion characteristics that produce stable behavior.

Future work with this particular injector element type should focus on the instability mechanism, more detailed measurement of mode shapes at key locations, and measurement of the Rayleigh index. If the injector dynamics are controlled primarily by intraelement processes, the differential response of the oxidizer and fuel flows to the oscillating pressure field and the means by which the fuel and oxidizer mix within the element to provide the initial conditions for unsteady combustion should be explored further.

Acknowledgements

This work was sponsored by NASA under Grant NCC8-200 and the School of Aeronautics and Astronautics at Purdue University. The authors wish to acknowledge the program management of Claudia Meyer and Jeff Rybak of NASA John H. Glenn Research Center, and technical input and support from Scott Meyer and Robert McGuire and Venkateswaran Sankaran of Purdue.

References

[1] Harrje, D. T., and Reardon, F. H. (eds.), *Liquid Propellant Rocket Combustion Instability*, SP-194, NASA, Washington, D.C., 1972.

[2] Culick, F. E. C., and Yang, V., "Overview of Combustion Instabilities in Liquid-Propellant Rocket Engines," *Liquid Rocket Engine Combustion Instability*, edited by V. Yang, and W. E. Anderson, Vol. 169, Progress in Aeronautics and Astronautics, AIAA, Washington, D.C., 1995, pp. 3–37.

[3] Combs, L. P., Hefner, R. J., Senneff, J. M., Harrje, D. T., Bloomer, H., Heidmann, M. F., Fairchild, D., Vincent, J., and Sokolowski, D. E., "Chapter 10: Stability Rating," *Liquid Propellant Rocket Combustion Instability*, edited by D. T. Harrje, and F. H. Reardon, SP-194, NASA, Washington, D.C., 1972.

[4] Dexter, C. E., Fisher, M. F., Hulka, J. R., Denisov, K. P., Shibanov, A. A., and Agarkov, A. F., "Scaling Techniques for Design, Development, and Test," *Liquid Rocket Thrust Chambers: Aspects of Modeling, Analysis, and Design*, edited by V. Yang, M. Habiballah, J. Hulka, and M. Popp, Vol. 200, Progress in Aeronautics and Astronautics, AIAA, Washington, D.C., 2004, pp. 553–600.

[5] Fisher, S. C., Dodd, F. E., and Jensen, R. J., "Scaling Techniques for Liquid Rocket Combustion Stability Testing," *Liquid Rocket Engine Combustion Instability*, edited by V. Yang, and W. E. Anderson, Vol. 169, Progress in Aeronautics and Astronautics, AIAA, Washington, D.C., 1995, pp. 545–564.

[6] Denisov, K. P., Kadishevich, A. S., Povolotzky, J. D., and Sarychev, F. G., "Full-Scale Component and Engine Stability Testing Using Spectral Analysis," *Liquid Rocket Engine Combustion Instability*, edited by V. Yang, and W. E. Anderson, Vol. 169, Progress in Aeronautics and Astronautics, AIAA, Washington, D.C., 1995, pp. 529–544.

[7] Penner, S. S., "On the Development of Rational Scaling Procedures for Liquid-Fuel Rocket Engines," *Jet Propulsion*, Vol. 27, No. 2, Feb. 1957, pp. 156–161.

[8] Penner, S. S., and Fuhs, A. E., "On Generalized Scaling Procedures for Liquid-Fuel Rocket Engines," *Combustion and Flame*, Vol. 1, No. 2, June 1957, pp. 229–240.

[9] Auble, C. M., "A Study of Injection Processes for Liquid Oxygen and Gaseous Hydrogen in a 200-Pound-Thrust Rocket Engine," NASA RM E56125a, Jan. 1957.

[10] George, D. J., "Rocket Injector Hot Firing and Cold Flow Spray Fields," AIAA Paper 73-1192, 1973.

[11] Cox, G. B., "Rocket Engine Injection Element Characterization," AIAA Paper 88-3135, 1988.

[12] Rahman, S. A., Pal, S., and Santoro, R. J., "Swirl Coaxial Atomization: Cold-Flow and Hot-Fire Experiments," AIAA Paper 95-381, 1995.

[13] Hulka, J., Schneider, J. A., and Davis, J., "Single Element Injector Testing for STME Injector Technology," AIAA Paper 92-3281, 1992.

[14] Beisler, M. A., Pal, S., Moser, M. D., and Santoro, R. J., "Shear Coaxial Injector Atomization in a LOX/GH2 Propellant Rocket," AIAA Paper 94-2775, 1994.

[15] Rahman, S. A., Cramer, J. M., Pal, S., and Santoro, R. J., "Coaxial Swirl Injector Studies at High O/F Ratios," *32nd JANNAF Combustion Subcommittee Meeting*, CPIA-PUB-631-VOL-II, Oct. 1995.

[16] Muss, J. A., Johnson, C. W., Cohn, R. K., Strakey, P. A., Bates, R. W., and Talley, D. G., "Swirl Coaxial Injector Development Part I—Test and Results," *38th JANNAF Combustion Subcommittee Meeting*, CPIA-PUB-712-VOL-I, 8–12 April 2002.

[17] Cohn, R. K., Strakey, P. A., Bates, R. W., Talley, D. G., Muss, J. A., and Johnson, C. W., "Swirl Coaxial Injector Development," AIAA Paper 2003-0124, 2003.

[18] Cohn, R. K., Danczyk, S. A., and Bates, R. W., "The Performance of Common and Advanced Hydrocarbon Fuels in a Uni-Element Combustor," *52nd JANNAF Propulsion Meeting*, JPM CD-04, 10–13 May 2004.

[19] Mayer, W., Schik, A., Schaffler, M., and Tamura, H., "Injection and Mixing Processes in High-Pressure Liquid Oxygen/Gaseous Hydrogen Rocket Combustors," *Journal of Propulsion and Power*, Vol. 16, No. 5, 2000, pp. 823–828.

[20] Miller, K. J., "Experimental Study of Longitudinal Instabilities in a Single Element Rocket Combustor," M.S. Thesis, School of Aeronautics and Astronautics, Purdue University, West Lafayette, IN, May 2005.

[21] Morgan, C. J., and Sokolowski, D. E., "Longitudinal Instability Limits with a Variable Length Hydrogen-Oxygen Combustor," NASA TN-D-6328, Washington, D.C., April 1972.

[22] Bazarov, V., "Influence of Stationary and Dynamic Parameters on High Frequency Combustion Stability," AIAA Paper 96-3119, 1996.

[23] Berman, K., and Logan, S. E., "Combustion Studies with a Rocket Motor Having a Full-length Observation Window," *ARS Journal*, Vol. 22, No. 2, March–April 1952, pp. 78–85.

[24] Berman, K., and Cheney, S. H., "Combustion Studies in Rocket Motors," *ARS Journal*, Vol. 23, No. 2, March–April 1953, pp. 89–96.

[25] Berman, K., and Cheney, S. H., "Rocket Motor Instability Studies," *Jet Propulsion*, Vol. 25, No. 10, Oct. 1955, pp. 513–518.

[26] Crocco, L., Grey, J., and Matthews, G. B., "Preliminary Measurements of the Combustion Time Lag in a Monopropellant Rocket Motor," *Proceedings of the Combustion Institute*, Vol. 5, 1955, pp. 164–170.

[27] Crocco, L., Grey, J., and Harrje, D. T., "On the Importance of the Sensitive Time Lag in Longitudinal High-Frequency Rocket Combustion Instability," *Jet Propulsion*, Vol. 28, No. 12, Dec. 1958, pp. 841–843.

[28] Zucrow, M. J., and Osborn, J. R., "An Experimental Study of High Frequency Combustion Pressure Oscillations," *Jet Propulsion*, Vol. 28, No. 10, Oct. 1958, pp. 649–654.

[29] Tsuji, H., and Takeno, T., "An Experimental Investigation on High-Frequency Combustion Oscillations," *Proceedings of the Combustion Institute*, Vol. 10, 1965, pp. 1327–1335.

[30] Long, M. R., Bazarov, V. G., and Anderson, W. E., "Main Chamber

Injectors for Advanced Hydrocarbon Booster Engines," AIAA Paper 2003-4599, 2003.
[31] Vasin, A. A., Kamensky, S. D., Katorgin, B. I., Kolesnikov, A. I., Nosov, V. P., Stavrulov, A. I., Fedorov, V. V., and Chvanov, V. K., U.S. Patent, US 6,244,041 B1, filed 12 June 2001.
[32] Canino, J. V., Heister, S. D., and Garrison, L., "Hydrodynamics Modeling of Oxidizer-Rich Staged Combustion Injector Flow," *52nd JANNAF Propulsion Meeting*, JPM CD-04, 10–13 May 2004.
[33] Cheng, G. C., Davis, R. R., Johnson, C. W., Muss, J. A., Greisen, D. A., and Cohn, R. K., "Development of GOX/Kerosene Swirl-Coaxial Injector Technology," AIAA Paper 2003-4751, 2003.
[34] Breisacher, K. J., "Axisymmetric Single Shear Element Combustion Instability Experiment," AIAA Paper 93-1953, 1993.
[35] Sisco, J. C., Austin, B. L., Mok, J. S., and Anderson, W. E., "Autoignition of Kerosene by Decomposed Peroxide in a Dump Combustor Configuration," *Journal of Propulsion and Power*, Vol. 21, No. 3, 2005, pp. 450–459.
[36] McBride, B. J., and Gordon, S., "Computer Program for Calculation of Complex Chemical Equilibrium Compositions and Applications," NASA, Ref. Pub. 1311, June 1996.
[37] Khavkin, Y., *The Theory and Practice of Swirl Atomizers*, Taylor and Francis, New York, 2004.
[38] Anon, *Guidelines for Combustion Stability Specifications and Verification Procedures for Liquid Propellant Rocket Engines*, CPIA Pub. No. 247, Laurel, MD, Oct. 1973.
[39] Kinsler, L. E., Frey, A. R., Coppens, A. B., and Sanders, J. V., *Fundamentals of Acoustics*, 4th ed., Wiley, New York, 2000.
[40] Sisco, J. C., Smith, R. J., Sankaran, V., and Anderson, W. E., "Examination of Mode Shapes in an Unstable Model Rocket Combustor," AIAA Paper 2006-4525, 2006.

V. Yang
Associate Editor